Sub-GHz Phase-Based Ranging System: Implementation and Evaluation

Masayoshi Oshiro[1] Shoji Otaka[1] Takayuki Kato[2] Katsuya Nonin[1] Masaki Nishikawa[1] Yoshiharu Nito[3]
Hideyuki Ishiwata[4] and Hiroshi Yoshida[1]

[1]Electronic Devices & Storage Research & Development Center, Toshiba Electronic Devices & Storage Corp., Kawasaki, Japan
[2]Broadcasting and Network Systems Dept., Toshiba Infrastructure Systems & Solutions Corp., Fuchu i, Japan
[3]Discrete Semiconductor Div., Toshiba Electronic Devices & Storage Corp., Kawasaki, Japan
[4]System Devices Div., Toshiba Electronic Devices & Storage Corp., Kawasaki, Japan
E-mail: {masayoshi.oshiro, shoji.ootaka, hiroshi7.yoshida}@toshiba.co.jp

Abstract—A prototype phase-detection ranging system based on the automotive remote / tele-control narrowband ARIB STD-T108 standard and operating in the sub-GHz band is designed, built, and evaluated. The prototype uses a pair of transceivers operating asynchronously. Problems with the frequency offset and initial phase are overcome by using an exchange sequence. The prototype employing 5.6MHz bandwidth achieves a distance error of 0.09 m under ideal environments without multipath and 0.88 m in outdoor conditions within the range of 6.0 m × 6.0 m area.

Keywords—Ranging; Relay Attack; Smart Key System; Multi-channel; Frequency Hopping

I. INTRODUCTION

In recent years, the demand for wireless location and ranging technology has increased and it is being adopted in many applications, particularly in the automotive field. Smart-key systems, which enable cars to be locked/unlocked and the engine to be started via a wireless authentication procedure between a car and a key fob, have been installed in many cars. However, with the introduction of these systems, the number of "relay attackers" [1] targeting security systems has also increased. In the relay attack shown in Fig. 1, an attacker A relays the authentication signal sent from a car at LF (Low Frequency) to another attacker B by up-converting the signal to RF (Radio Frequency). Then, attacker B sends the signal to the key fob by down-converting the relayed signal to LF. The key fob sends back an acknowledge response intended for the car. In the attack, the smart-key system is fooled into thinking that the key fob is close to the car. Current smart-key systems are known to be vulnerable to such attacks [2]. Therefore, a countermeasure technique that can detect whether a car and a key fob are actually close or not is required.
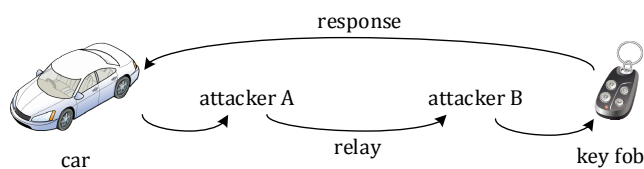

Fig. 1. Typical relay attack for smart key system

There are various candidates for distance measurement techniques, such as a received signal strength indication (RSSI) detection method [3], an impulse method [4], a frequency-modulated continuous-wave (FMCW) method [5], and a phase-detection method [6][7]. These techniques have various advantages and disadvantages. Of these, the RSSI-based detection method is the least accurate. Furthermore, with smart-key systems, an integrated circuit using the impulse method or the FMCW method consumes more than the other methods. A phase-detection method can be easily configured in terms of circuit size and power consumption. Therefore, the phase-detection method using two-frequency [6] is selected for the prototype.

A sub-GHz band ranging technology compliant with the automotive remote / tele-control narrowband ARIB STD-T108 standard [8] is introduced in this paper. The technology measures distance between a car and a key fob and operates in the of 920-MHz frequency band, which is more advantageous than the 2.4-GHz band such as Bluetooth® in terms of propagation loss.

Generally, systems that handle reflected waves such as a radar can be configured to have perfect synchronization because the local signal source of the transmitter and receiver is identical. However, an asynchronous system, which consists of two independent transceivers, has been adopted for the prototype. Our prototype overcomes performance degradation caused by the frequency offset and initial phase, which are inherent issues in asynchronous systems, by using an exchange sequence. Furthermore, as delay variation in the RF chain due to gain change causes significant distance error in the phase-detection system, a calibration technique to compensate for the delay at each gain has been introduced.

To verify the performance of the ranging technique, the prototype was evaluated in various environments: an ideal environment without multipath, an outdoor environment, and an outdoor environment with a car-mounted antenna.

In this paper, the measurement principle and the basic ranging algorithm are presented in Section II, the prototype configuration and calibration method are described in Section III, and the measurement results are reviewed in Section IV.

II. RANGING PRINCIPLE OF PHASE-DETECTION

This section describes the principle of two-frequency phase detection. The distance d is calculated using (1) if the phase difference between the two frequencies is within 2π.

$$d = \left| \frac{c\,(\theta_{f2} - \theta_{f1})}{2\pi(f_2 - f_1)} \right| \qquad \text{c: light speed} \qquad (1)$$

where f_1 and f_2 are CW frequencies and θ_{f1} and θ_{f2} are measured phase on f_1 and f_2, respectively.

A. Ideal case without frequency offset

The principle of using an exchange sequence for ranging is described below.

The initial phase is inherently canceled by making a round trip even if the two nodes are not synchronized [9]. As shown in

Fig. 2, a single-tone signal is sent from an initiator to a reflector and it is then sent back from the reflector to the initiator. It is assumed that the initial phase of each local reference is different.

The detailed procedure is described below.

The initiator transmits a signal $\cos(2\pi f_1 t + \theta_{i1A})$, where θ_{i1A} is the initial local phase of the initiator at frequency f_1. The reflector receives the transmission signal $\cos(2\pi f_1 t + \theta_{i1A} - 2\pi f_1\tau)$, where τ is the time delay between the initiator and the reflector. Baseband signal $s_{f1B}(t)$ is obtained by mixing the transmission signal from the initiator with the local signal of the reflector.

$$s_{f1B}(t) = \cos(2\pi f_1 t + \theta_{i1A} - 2\pi f_1\tau) \times \cos(2\pi f_1 t + \theta_{i1B})$$

$$= \frac{1}{2}\cos(4\pi f_1 t + \theta_{i1A} + \theta_{i1B} - 2\pi f_1\tau) + \frac{1}{2}\cos(\theta_{i1A} - \theta_{i1B} - 2\pi f_1\tau) \quad (2)$$

where θ_{i1B} is the initial local phase of the reflector at frequency f_1. Then, the phase of the received signal θ_{f1B} in (3) is extracted from the second term of the above equation and calculated at the reflector.

$$\theta_{f1B} = \theta_{i1A} - \theta_{i1B} - 2\pi f_1\tau \quad (3)$$

Similarly, phase θ_{f1A} in (4) is also calculated at the initiator.

$$\theta_{f1A} = \theta_{i1B} - \theta_{i1A} - 2\pi f_1\tau \quad (4)$$

The initial phase is canceled by calculating phase θ_{f1_2way} in (5).

$$\theta_{f1\_2way} = \theta_{f1B} + \theta_{f1A} = -4\pi f_1\tau \quad (5)$$

Next, the same procedure is followed for f_2 in order to calculate θ_{f2B}, θ_{f2A}, and θ_{f2_2way} in (6).

$$\theta_{f2\_2way} = \theta_{f2B} + \theta_{f2A} = -4\pi f_2\tau \quad (6)$$

From above procedure, the phase differences between the initiator and the reflector for f_1 and f_2 are obtained from (5) and (6), respectively. The distance d is calculated by removing τ from (7) and (8) as shown in (9).

$$\theta_{f2\_2way} - \theta_{f1\_2way} = -4\pi(f_2 - f_1)\tau \quad (7)$$

$$\tau = \frac{d}{c} \quad (8)$$

$$d_{2way} = \left| \frac{c\,(\theta_{f2\_2way} - \theta_{f1\_2way})}{4\pi(f_2 - f_1)} \right| \quad (9)$$

To obtain the total phase difference for each frequency, the phase information of θ_{f1B} and θ_{f2B}, which are observed at the reflector, are sent to the initiator.

As described above, even in an asynchronous system, the initial local phase difference between the initiator and the reflector is canceled in a round trip sequence by using the f_1 and f_2 frequencies.

B. Actual case applying time sequencal procedure with frequency offset

The round-trip exchange sequence can cancel the initial phase difference as described in section A. However, the distance accuracy is degraded by frequency offset between the initiator and the reflector in the actual case. So, we propose the cancellation technique of the phase error due to the frequency offset.

We assume frequency offset Δf_1 between the reflector and the initiator. Phase θ_{f1B} including Δf_1 is extracted at the reflector by the same calculation as described in (3).

$$\theta_{f1B} = \theta_{i1A} - \theta_{i1B} - 2\pi f_1\tau - 2\pi\Delta f_1 t \quad (10)$$

The reflector transmits return signal with an interval of T from the initiator transmission. Then the initiator receives the signal $\cos\{2\pi(f_1 + \Delta f_1)(t + T) + \theta_{i1B} - 2\pi(f_1 + \Delta f_1)\tau\}$. Similarly, phase θ_{f1A} is also calculated at the initiator.

$$\theta_{f1A} = 2\pi\Delta f_1 t + 2\pi\Delta f_1 T + \theta_{i1B} - \theta_{i1A} - 2\pi(f_1 + \Delta f_1)\tau \quad (11)$$

Then, the round-trip phase θ_{f1_2way} is given by (12).

$$\theta_{f1\_2way} = \theta_{f1B} + \theta_{f1A} = -4\pi f_1\tau + 2\pi\Delta f_1 T - 2\pi\Delta f_1\tau \quad (12)$$
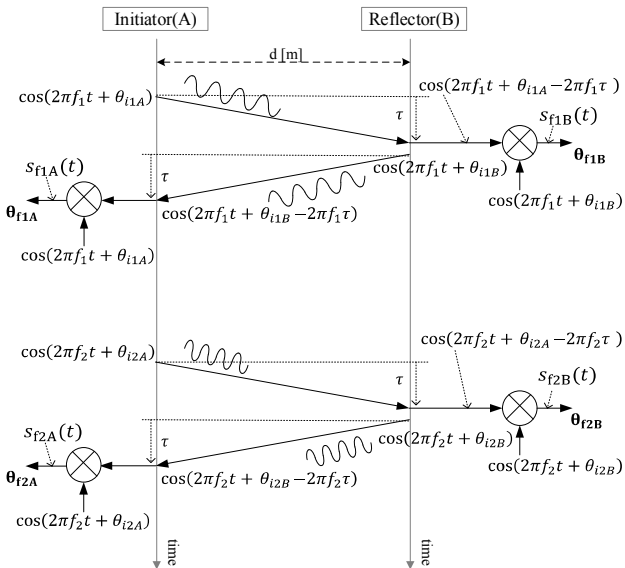

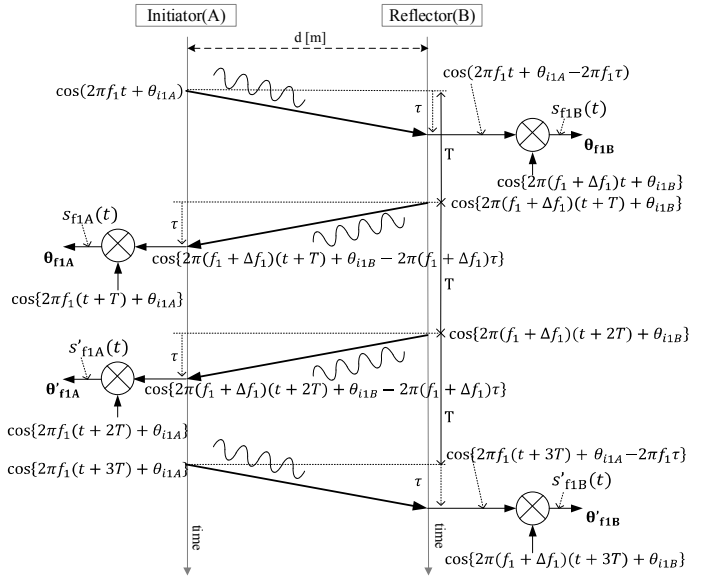Fig. 2.   Ranging principle of two-frequency phase detection

Fig. 3.   Ranging principle introducing reverse sequence for frequency f_1

In (12), the second and third terms including Δf1, which are to be canceled for measurement accuracy, is added to (5). In order to cancel these terms, we introduce an additional reverse sequence for the two frequencies as shown in Fig.3.

Here, two phases θ'_{f1A} and θ'_{f1B} are extracted by (13), (14).

$$\theta'_{f1A} = 2\pi\Delta f_1 t + 2\pi\Delta f_1 2T + \theta_{i1B} - \theta_{i1A} - 2\pi(f_1 + \Delta f_1)\tau \quad (13)$$

$$\theta'_{f1B} = \theta_{i1A} - \theta_{i1B} - 2\pi f_1\tau - 2\pi\Delta f_1 t - 2\pi\Delta f_1 3T \quad (14)$$

Then, the round-trip phase θ'_{f1_2way} is given by (12).

$$\theta'_{f1\_2way} = \theta'_{f1B} + \theta'_{f1A} = -4\pi f_1\tau - 2\pi\Delta f_1 T - 2\pi\Delta f_1\tau \quad (15)$$

Introducing the reverse sequence, $2\pi\Delta f_1 T$ is canceled by adding four phases i.e., (10), (11), (13), (14) in (16).

$$\theta_{f1\_4way} = \theta_{f1\_2way} + \theta'_{f1\_2way} = \theta_{f1B} + \theta_{f1A} + \theta'_{f1B} + \theta'_{f1A}$$
$$= -8\pi f_1\tau - 4\pi\Delta f_1\tau \quad (16)$$

However, it should be noted that $-4\pi\Delta f_1\tau$ in the second term still remains.

In order to calculate θ_{f1_4way}, the same procedure is applied for f_2 as for f_1 in Fig. 3 with start time of D.
The four phases $\theta_{f2B}, \theta_{f2A}, \theta'_{f2A}, \theta'_{f2B}$ are given by (17).

$$\theta_{f2B} = \theta_{i2A} - \theta_{i2B} - 2\pi f_2\tau - 2\pi\Delta f_2(D + t)$$
$$\theta_{f2A} = 2\pi\Delta f_2 t + 2\pi\Delta f_2(D + T) + \theta_{i2B} - \theta_{i2A} - 2\pi(f_2 + \Delta f_2)\tau$$
$$\theta'_{f2A} = 2\pi\Delta f_2 t + 2\pi\Delta f_2(D + 2T) + \theta_{i2B} - \theta_{i2A} - 2\pi(f_2 + \Delta f_2)\tau$$
$$\theta'_{f2B} = \theta_{i2A} - \theta_{i2B} - 2\pi f_2\tau - 2\pi\Delta f_2 t - 2\pi\Delta f_2(D + 3T) \quad (17)$$

where θ_{i2A} is the initial local phase of the initiator, and θ_{i2B} is the initial local phase of the reflector at frequency f_2.
Similarly, $2\pi\Delta f_2 T$ is also canceled by adding four phases in (18).

$$\theta_{f2\_4way} = \theta_{f2B} + \theta_{f2A} + \theta'_{f2B} + \theta'_{f2A}$$
$$= -8\pi f_2\tau - 4\pi\Delta f_2\tau \quad (18)$$

Finally, subtracting $\theta_{f1_{4way}}$ from $\theta_{f2_{4way}}$ obtains two terms in (19).

$$\theta_{f2\_4way} - \theta_{f1\_4way} = -8\pi(f_2 - f_1)\tau - 4\pi(\Delta f_2 - \Delta f_1)\tau \quad (19)$$

Though the second term in (19) is still remained, little degradation will be expected; when $\Delta f_2 - \Delta f_1$ is 100 ppm of 5.6 MHz, i.e., 560 Hz, and τ is 33ns, i.e., 10 m, the second term will be 0.013 degrees, i.e., 0.002 m, which can be considered as negligibly small.

Thus, the distance d is calculated by removing τ from (19) and (8) as shown in (20).

$$d_{4way} = \left| \frac{c\,(\theta_{f2\_4way} - \theta_{f1\_4way})}{8\pi(f_2 - f_1)} \right| \quad (20)$$
$$(0 \le \theta_{f2_{4way}} - \theta_{f1_{4way}} < 4\pi)$$

As described in this section, the effect of the frequency offset is canceled by applying the exchange sequence.

III. PROTOTYPE CONFIGURATION

Fig. 4 shows the configuration of the prototype. Two units are configured to implement the ranging system by introducing an exchange sequence controlled by PCs via UART. An AD9361 [10] is used as the RF transceiver, and digital signal processing is implemented using a Virtex-7 [11].

Table I shows the specification of the prototype, which operates in the 920-MHz band and is compliant with ARIB STD-T108. The frequencies assigned for two-tone operation are 922.4 MHz and 928.0 MHz.

Three major techniques are applied in the prototype: optimization of parameter setting; phase exchange sequencing; and calibration to allow for delay variation in the RF chain. These are described in detail below.

TABLE I.   SPECIFICATION OF THE PROTOTYPE

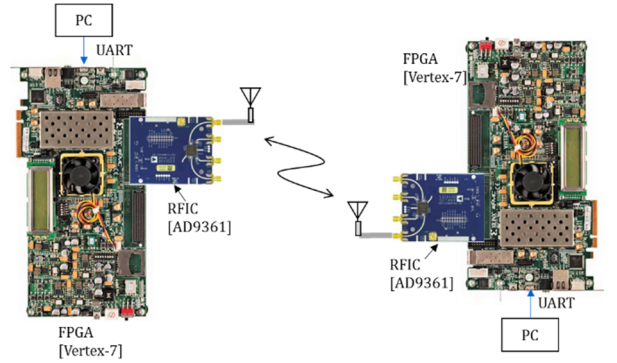| Item	Table
Ranging method	two-frequency phase detection
RF	922.4MHz, 928.0MHz
Local frequency	924.0MHz
TX power	0dBm
RFIC	AD9361
FPGA	Xilinx Virtex-7

Fig. 4.   Prototype configuration

A. Optimization of parameter setting

In terms of propagation loss, it is preferable to select a low carrier frequency. The 920-MHz band as set out in ARIB-T108 is sufficiently low compared with other candidates such as Bluetooth® that operate in the 2.4-GHz band.

In a two-frequency phase-detection system, the frequency difference between two tones should be carefully selected.

In terms of measurement error, the frequency difference should be wide enough to suppress the effect of signal-to-noise ratio (SNR) and at the same time it should be narrow enough to extend the ranging limit. Since the variance of the phase is equivalent to SNR, the distance error is given by (21).

$$\text{Distance error} = \frac{c}{2\pi(f_2 - f_1)} * 10^{(-SNR/20)} \quad (21)$$

Fig. 5 shows theoretical standard deviation of the distance error versus the frequency difference of two frequencies at an SNR of 20 dB. The prototype is designed such that it has a frequency difference of 5.6 MHz so that the distance error is sufficiently low, that is, less than 1 m at an SNR of 20 dB.

As the upper limit of the measurement range d_{max} is determined by (10), the ranging limit is 26.7 m, which is a sufficient range for relay attacks, at 5.6 MHz.

$$d_{max} = \left| \frac{c}{2(f_2 - f_1)} \right| \qquad (22)$$

Fig. 6 shows the theoretical and measured standard deviation of the distance error versus received signal power. The theoretical distance error in Fig. 6 is calculated by (21) under the condition that SNR of 20dB is expected with RSSI of −100dBm. The measured result shows good agreement with the theoretical value to be revealed that the prototype has sufficient performance for distance measurement.
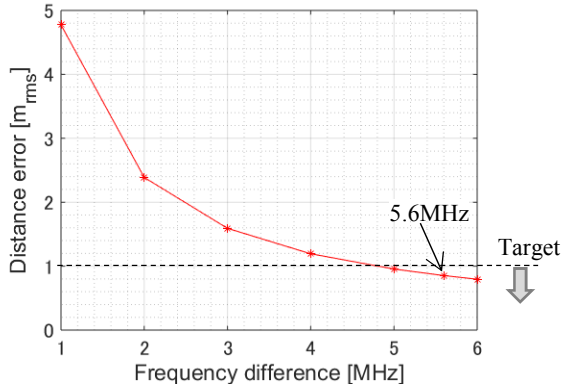

Fig. 5.   Distance error V.S. frequency difference of two-tone at SNR of 20dB
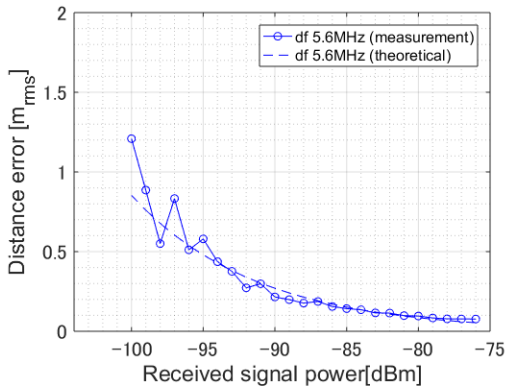

Fig. 6.   Distance error V.S. received signal power

B. Fixed exchange sequence

Cancellation mechanism of frequency offset between the initiator and the reflector based on a mathematical model is shown in section II. Detailed timing chart of the proposed exchange sequence is described in this section.

Fig. 7 shows an outline of the operation timing. The fixed exchange sequence is described below, in which the procedure is started with a transmission signal from the initiator so as not to require any external trigger.

The flow of the procedure is as follows;

1. The initiator and the reflector are set to the first frequency f_1.
2. The initiator starts transmission of the CW to the reflector.

3. The measurement sequence at the reflector starts at the detection of the CW from the initiator after a propagation delay of τ seconds.
4. The reflector samples the phase θ_{f1B} a fixed time after detection of the initiator's signal.
5. The reflector sends back the CW to the initiator a fixed time after the phase sampling timing in the procedure 4.
6. The initiator samples the phase θ_{f1A} a fixed time after the start of the CW transmission. The sampling starts without detecting the send-back CW from the reflector.
7. With the same procedure as 6, the initiator samples the phase θ'_{f1A} a fixed time after the start of the CW transmission.
8. The reflector samples the phase θ'_{f1B} a fixed time after the start of the CW transmission. The sampling starts without detecting the send-back CW from the initiator.
9. The initiator and the reflector are switched to the second frequency f_2 to sample phases by the same sequence (repeat steps 2-8).
10. The sampled phase information in the reflector ($\theta_{f1B}, \theta'_{f1B}, \theta_{f2B}, \theta'_{f2B}$) is transferred to the initiator using ASK modulation.

In the above procedure, no synchronization process is required due to short operation periods so as not to miss-reception of coming CW.

By using above procedure, the initial phase difference and frequency offset between the initiator and the reflector is canceled.
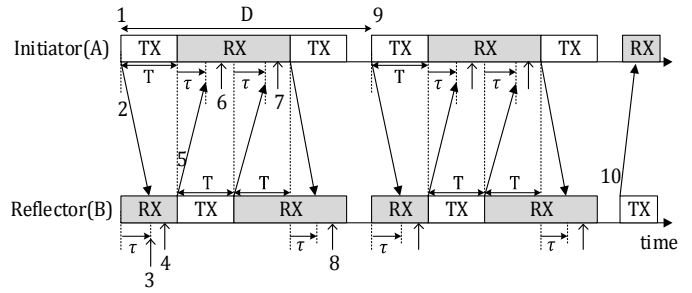

Fig. 7.   Timing chart (Fixed exchange sequence)

C. Calibration to compensate for delay variation in the RF chain

With a phase-detection method, even if the fixed delay is compensated for perfectly, a distance error still occurs due to delay variation in the RF chain. Generally, the delay variation occurs when an LNA (low-noise amplifier) or a VGA (variable-gain amplifier) gain is changed using AGC (automatic gain control) as shown in the block diagram of Fig. 8. Therefore, it is necessary to estimate the amount of delay for each RX gain to correct the measured distance.

In the calibration procedure, first an antenna port of the initiator and an antenna port of the reflector are directly connected, as shown in Fig. 8. Then RX gain is set to a minimum and TX power is set to a predetermined value.

Next, the amount of delay for the direct connection is estimated and stored as the compensation distance.

Secondly, TX attenuation and RX gain are increased in 1 dB steps simultaneously to extract the compensation distance for each RX gain (11).

The estimated distance is calculated by subtracting the compensation distance corresponding to the RX gain from the measurement distance, as shown in (12).

$$d_{each\ RXgain} = \left| \frac{c\left(\theta_{f2\_direct\_connect} - \theta_{f1\_direct\_connect}\right)}{4\pi(f_2 - f_1)} \right| \quad (23)$$

$$d_{est\_distance} = d_{meas} - d_{each\ RXgain} \quad (24)$$

Fig. 9 shows the measured compensation distance for each gain. These results show that it is necessary to correct the measured distance since the error due to the gain change is large (approximately 1.5 m).
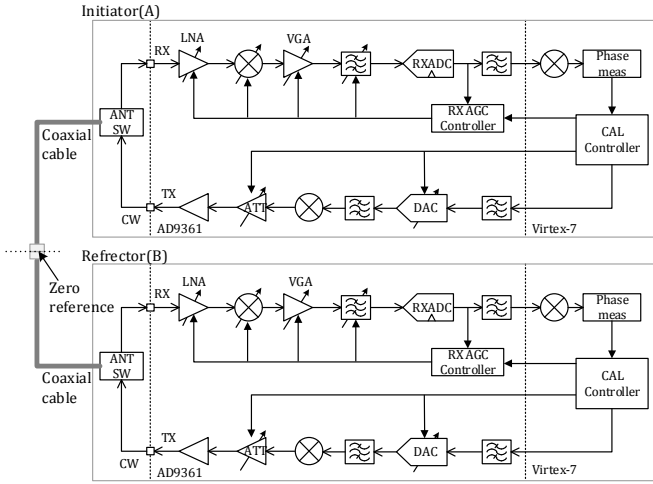

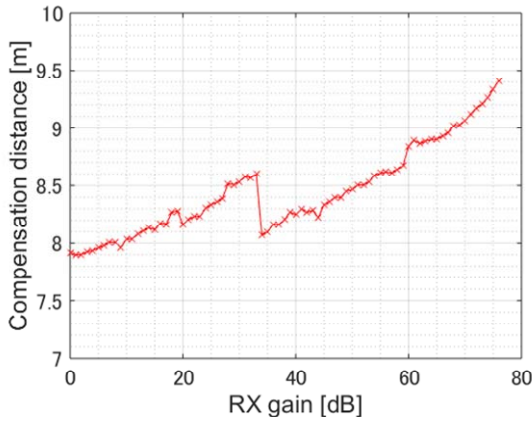Fig. 8.   Block diagram of the ranging system for initial calibration

Fig. 9.   Compensation distance for each gain

IV. MEASUREMENT RESULTS

The performance of the prototype at measuring distance was evaluated in the following three steps:

First, to confirm the performance of the prototype, an evaluation was performed in an anechoic chamber to eliminate the effect of multipath (A).

Next, to evaluate real-environment performance, the prototype measured distances under two outdoor conditions: (B) with line of sight (LOS) and (C) with partial non-line of sight (NLOS) to a car-mounted antenna.

A. Anechoic chamber

A pair of opposing antennas attached to the prototypes were placed along a straight line to measure distances from 1 to 5 m in 1-m steps. The averaged estimated distance and error between the estimated distance and the actual distance at each position are shown in Fig. 10. Under this condition, high accuracy was achieved with errors within +/− 25 cm, which reveals SNR of the received signal is around 31 dB.
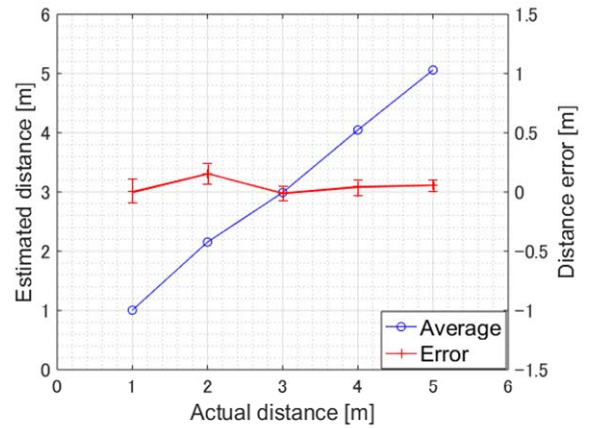This result includes degradation factors due to the actual wireless environment.

Fig. 10. Estimated distance and distance error in anechoic chamber

B. Outdoor conditions

In the outdoor LOS environment as shown in Fig. 11, the distance between one antenna placed at coordinates (0 m, 0 m) with the other placed at each grid point was measured. The grid was 6 m × 6 m with 50-cm spacing. The antenna for each prototype was placed at a height of 80 cm.

Fig. 12 (a) shows the estimated distance, and Fig. 12 (b) shows the error between the estimated distance and the actual distance. The results show that the distance errors are almost all within 2 m for all the measurement positions in this area.
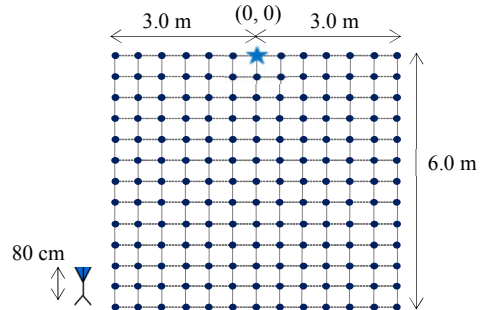

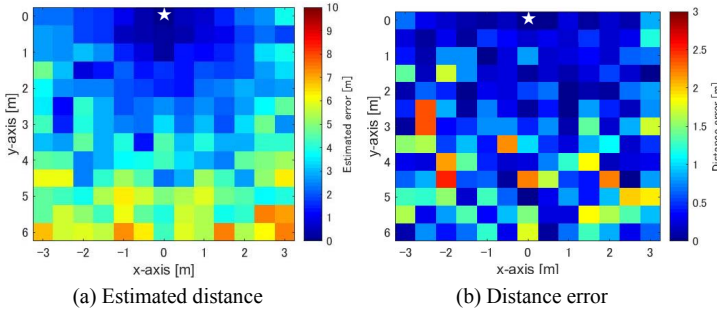Fig. 11. Measured position under outdoor condition

(a) Estimated distance   (b) Distance error

Fig. 12. Estimated distance and distance error in outdoor w/o car

C. Outdoor conditions with a car-mounted antenna

In this evaluation, the distance between one antenna attached to the car and the other antenna at each grid point was measured. The antenna for the car was attached at a door handle or at the trunk, while the other antenna was placed at each grid point shown in Fig. 13.

The grid consisted of an x-axis [− 4.5 m, + 4.0 m] and a y-axis [0 m, 5.0 m] with 50-cm spacing. The two antennas were placed at a height of 80 cm. The car was placed at the position shown in Fig. 13.

Figs. 14 (a) and 14 (b) show the estimated distance and the error between the estimated distance and the actual distance at each grid point with the antenna attached at the door handle (0 m, 1.5 m). The LOS area is 1.5 m to 5.0 m on the y-axis.

As shown in the figures, the accuracy in the LOS area is high, with distance measurement error of within 2 m. However, the accuracy in the NLOS area is not high due to the large phase variation caused by multipath.
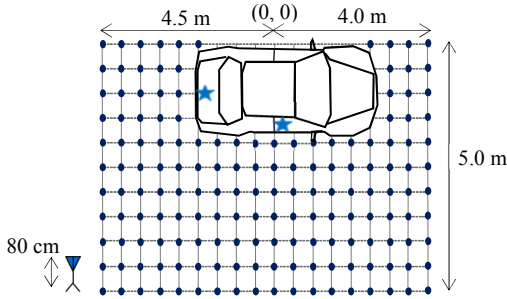

Fig. 13. Measured position under outdoor conditions with a car

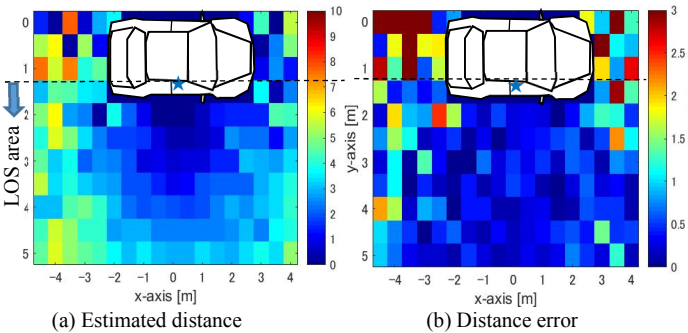(a) Estimated distance   (b) Distance error

Fig. 14. Estimated distance and distance error w/ car with antenna at door handle

Figs. 15 (a) and 15 (b) show the estimated distance and the error when the antenna was attached at the trunk (− 2.0 m, 1 m).

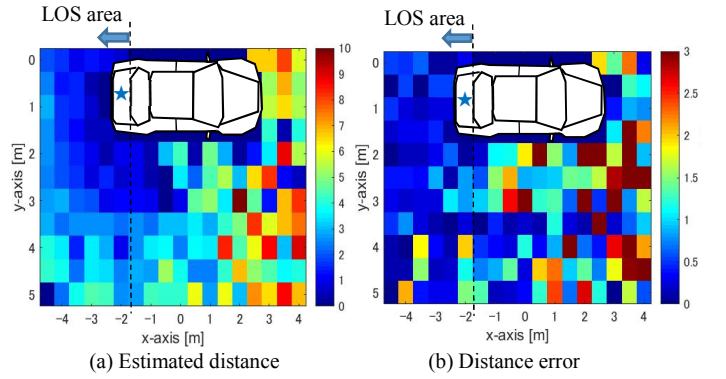(a) Estimated distance   (b) Distance error

Fig. 15. Estimated distance and distance error w/ car with antenna at trunk

TABLE II.   RESULT SUMMARY (LOS AREA)

Condition	Anechoic Chamber (A)	Outdoor (B)	Outdoor with car (C)
Accuracy within 2m error	100%	95.8%	Door 97.0 % Trunk 96.8 %
Maximum error	0.25 m	2.50 m	Door 2.86 mrms Trunk 2.07 mrms
Distance error	0.09 mrms	0.88 mrms	Door 0.75 mrms Trunk 0.64 mrms

Table II shows a summary of the evaluation results in the LOS area. The results show that a distance error within 2 m was achieved over 95% accuracy.

Figs 14 and 15 show that each other's NLOS areas are complementary so that introducing diversity technique using both antennas decreases total NLOS area to improve the accuracy. Therefore, these measured results demonstrate that high accuracy measurement is possibly an effective countermeasure against relay attacks.

V. CONCLUSION

This paper has described a prototype phase-detection ranging system compliant with ARIB STD-T108 using the sub-GHz band. Three key techniques were applied: optimization of parameter setting; phase exchange sequencing; and calibration to allow for delay variation in the RF chain. These allow the prototype to provide high-accuracy measurement. The evaluation results demonstrate that the prototype has sufficient accuracy to be used as a countermeasure against relay attacks.

On the other hand, some future issues, such as narrow ambiguity range and degradation due to multipath, are remained. Introducing narrower bandwidth could enhance the maximum distance and employing multiple frequencies could contribute to obtain channel impulse response.

REFERENCES

[1] A. Alrabady and S. Mahmud. "Some attacks against vehicles' passive entry security systems and their solutions", Vehicular, Technology, IEEE Transactions on, 52(2): 431-439, Mar. 2003.

[2] A. Ranganathan, S. Capkun, "Are We Really Close? Verifying Proximity in Wireless Systems", IEEE Security & Privacy, Jun. 2017.

[3] J. J. Wang, J. G. Hwang, J. G. Park. "A novel indoor ranging method using weighted altofrequent RSSI measurements", 2017 11th International Conference on Signal Processing and Communication Systems (ICSPCS), Dec. 2017.

[4] Jerzy Kolakowski, "Application of phase information for TOA determination in UWB direct conversion receivers," International Conference on Indoor Positioning and Indoor Navigation, Oct. 2016.

[5] M. I. Skolnik, "Introduction to Rader System", McGraw-Hill, New York. 1962.

[6] G. von Zengen, Y. Schroeder, S. Rottmann, F. Buesching, and L. C. Wolf, "No-cost distance estimation using standard WSN radios," IEEE The 35th Annual IEEE International Conference on Computer Communications (INFOCOM 2016), 2016.

[7] F. Wolf, J.-B. Dore, X. Popon, S. de Rivaz, F. Dehmas,and J.-P. Cances, "Coherent Multi-Channel Ranging for Narrowband LPWAN: Simulation and Experimentation Results," IEEE 15th Workshop on Positioning, Navigation and Communications (WPNC), 2018.

[8] ARIB STD-T108, v1.3, Apr. 2019,
[Online]. Available: http://www.arib.or.jp

[9] F. L. Beckner, Darrell K "RANGING BY SEQENTIAL TONE TRANSMISION", US Patent 5,220,332, Jun. 1993.

[10] Analog Devices "AD9361 datasheet, Rev.F", Nov, 2016,
[Online]. Available: https://www.analog.com

[11] Xilinx "Vertex-7 datasheet, Rev.2.6", Feb, 2018,
[Online]. Available: https://www.xilinx.com